Contrasting coordination behavior of Group 12 perchlorate salts with an acyclic N_3O_2 donor ligand by X-ray crystallography and ^{1}H NMR

Daniel B. Tice, Robert D. Pike, Deborah C. Bebout*

Department of Chemistry, The College of William & Mary, Williamsburg, VA 23188

ELECTRONIC SUPPLEMENTARY INFORMATION

Table of Contents with Abbreviated Descriptions	Page

Table S1. Hydrogen bonds for [Zn(**L1**)(OH_2)](ClO_4)$_2$ (**1**) [Å and °].

D-H...A	d(D-H)	d(H...A)	d(D...A)	<(DHA)
O(1W)-H(1W)...O(3)#1	0.71(3)	2.57(3)	3.148(2)	140(3)
O(1W)-H(1W)...O(4)#1	0.71(3)	2.17(3)	2.848(3)	162(3)
O(1W)-H(2W)...O(10)#1	0.88(3)	1.84(3)	2.715(2)	162(3)

Symmetry transformations used to generate equivalent atoms: #1 x-1/2,-y+1/2,z-1/2

Table S2. Hydrogen bonds for [Cd(**L1**)(OH_2)(ClO_4)](ClO_4) (**2**) [Å and °].

D-H...A	d(D-H)	d(H...A)	d(D...A)	<(DHA)
O(1W)-H(1W)...O(7)#1	0.76(3)	2.02(3)	2.750(3)	160(3)
O(1W)-H(2W)...O(8)	0.76(3)	2.04(3)	2.801(3)	175(3)

Symmetry transformations used to generate equivalent atoms: #1 x-1/2,y,-z+1/2

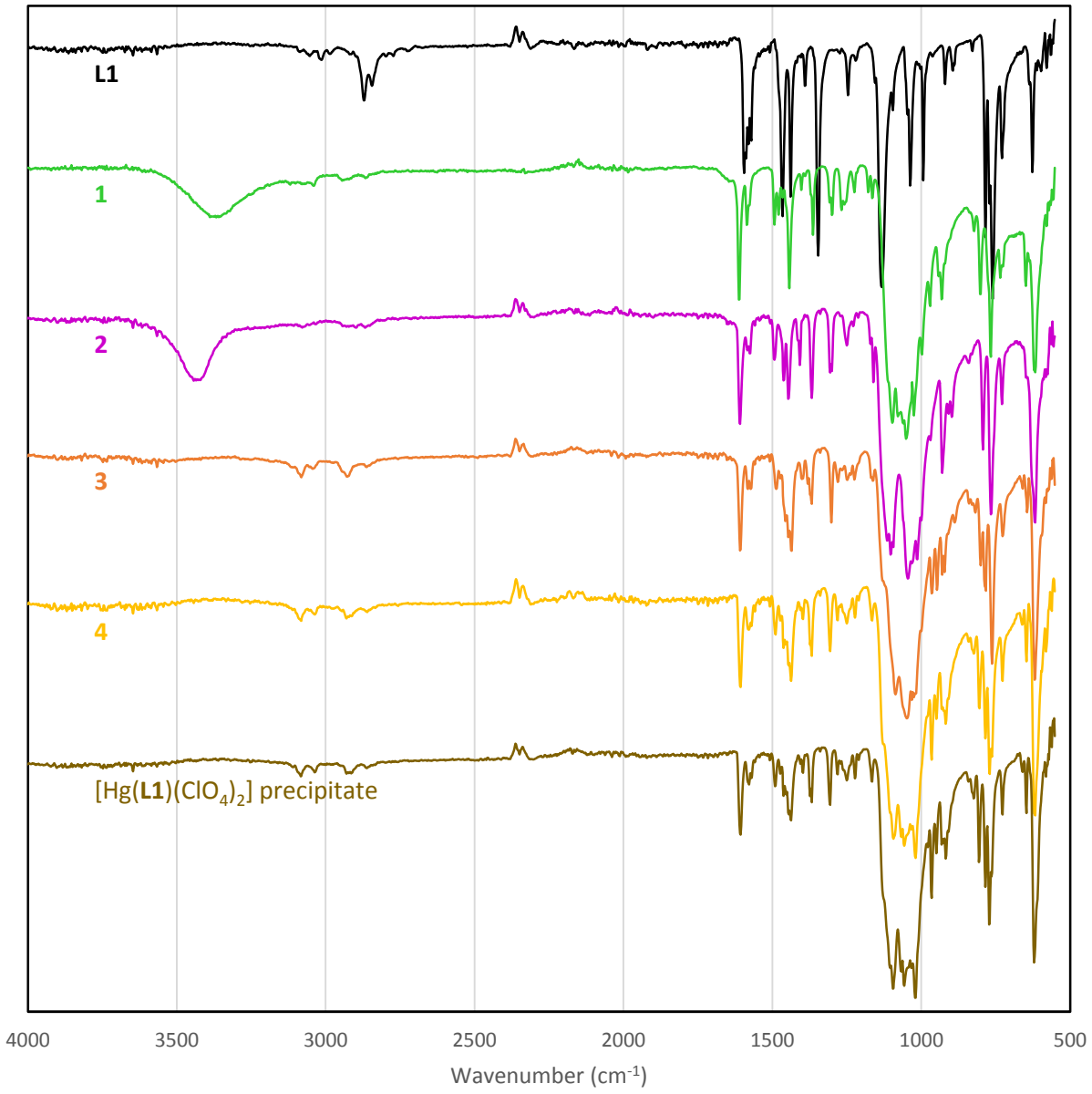

Figure 1. FTIR spectra of crystalline [Zn(**L1**)(OH_2)](ClO_4)$_2$ (**1**), [Cd(**L1**)(OH_2)($OClO_3$)](ClO_4) (**2**), [Hg(**L1**)(κ^2-ClO_4)$_2$]$_2$ (**3**), [Hg(**L1**)(κ^2-ClO_4)($OClO_3$)]$_2$ (**4**) and [Hg(**L1**)(ClO_4)$_2$] precipitated from acetonitrile/m-xylene.

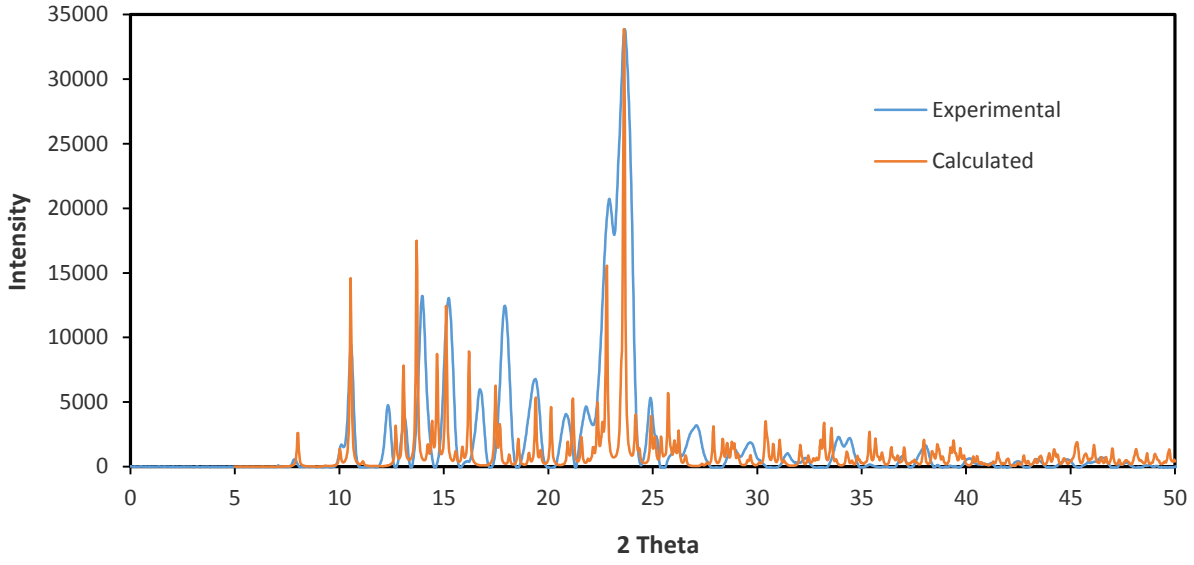

Figure S2. Powder diffraction analysis of crystalline [Zn(**L1**)(OH_2)](ClO_4)$_4$ (**1**). Experimental data (blue) for the bulk crystalline material prepared by slow evaporation from an acetonitrile/mesitylene solution containing stiochiometrically equivalent amounts of **L1** and Zn(ClO_4)$_2$ compared to the calculated (Mercury 3.3) powder pattern for **1** (orange). Experimental 2θ peaks 11.66, 11.88, 13.64, and 13.78° poorly accounted for by experimental data

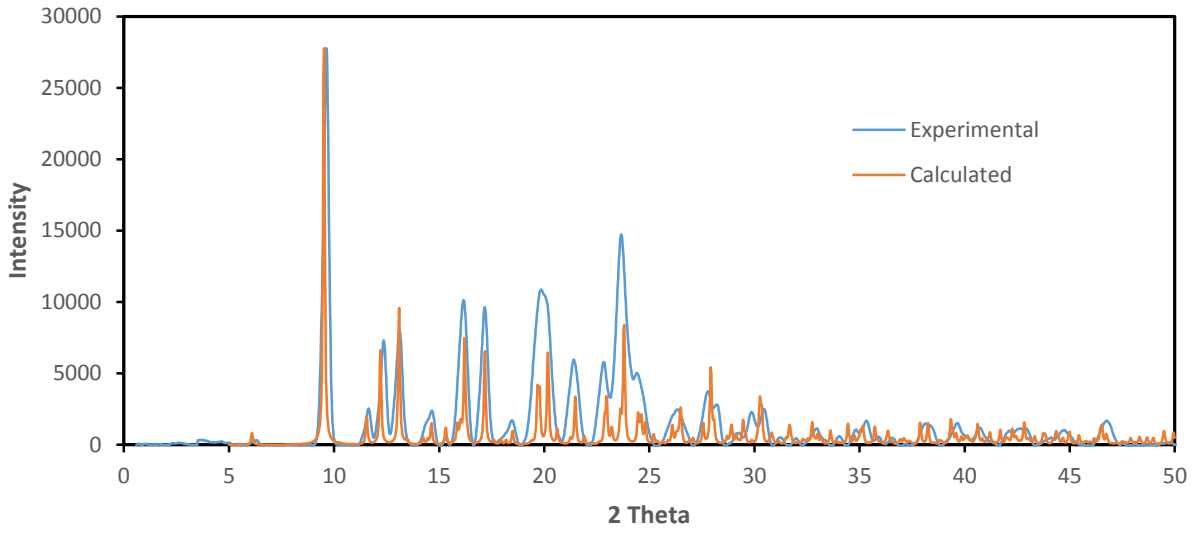

Figure S3. Powder diffraction analysis of crystalline [Cd(**L1**)(OH_2)($OClO_3$)](ClO_4) (**2**). Experimental data (blue) for the crystalline material prepared by slow evaporation of an acetonitrile/m-xylene solution containing stiochiometrically equivalent amounts of **L1** and Cd(ClO_4)$_2$ is compared to the calculated (Mercury 3.3) powder pattern for **2** (orange).

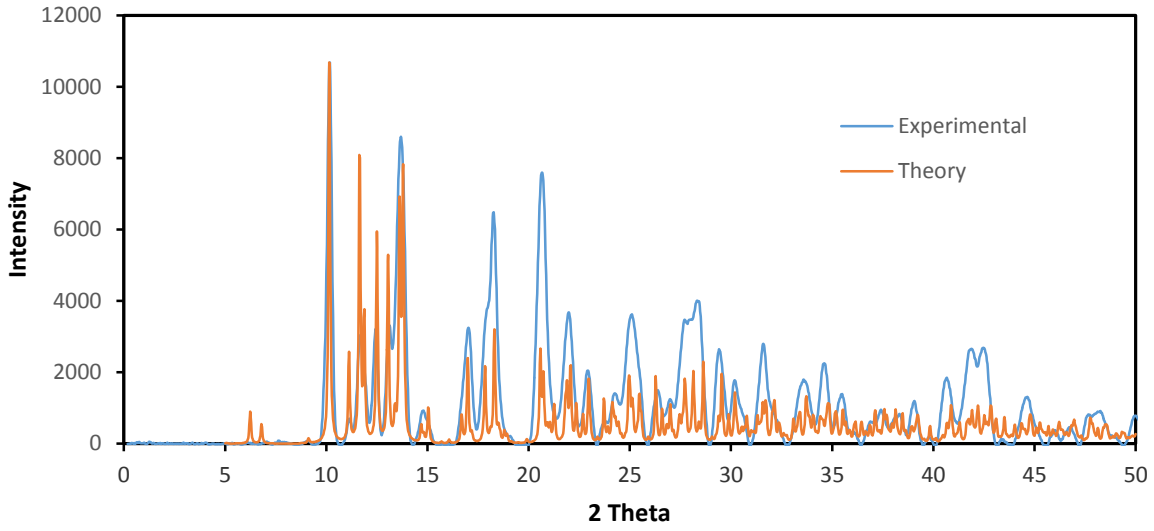

Figure S4. Powder diffraction analysis of crystalline [Hg(**L1**)(κ^2-ClO_4)$_2$] (**3**). Experimental data (blue) for the crystalline material prepared by slow evaporation of an acetonitrile/m-xylene solution containing stiochiometrically equivalent amounts of **L1** and $Hg(ClO_4)_2$ compared to the calculated (Mercury 3.3) powder pattern for **3** (orange).

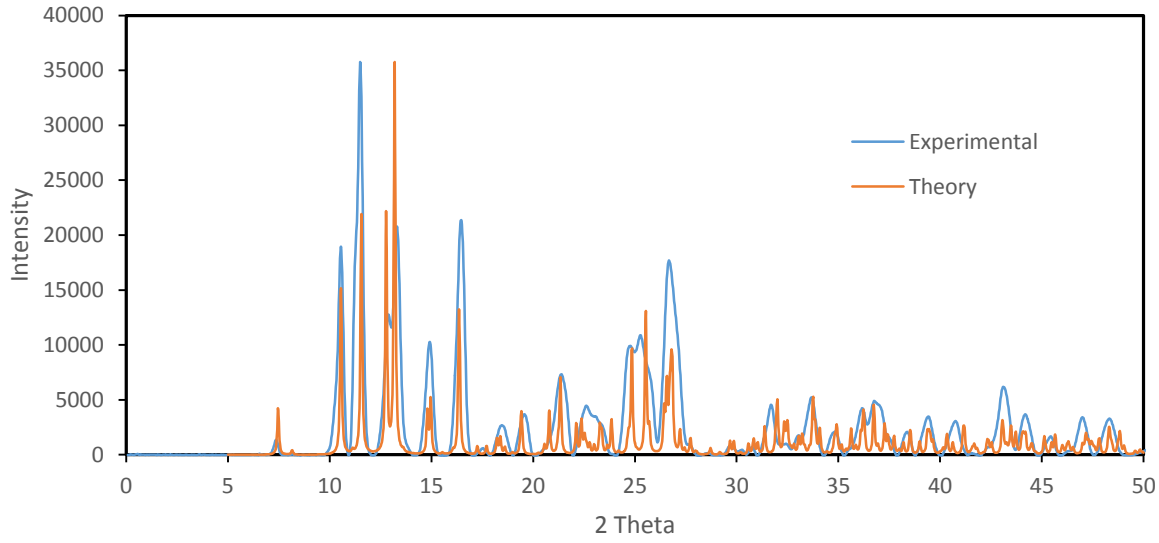

Figure S5. Powder diffraction analysis of crystalline [Hg(**L1**)(κ^2-ClO_4)($OClO_3$)] (**4**). Experimental data (blue) for **4** prepared by slow evaporation of an acetone solution containing stiochiometrically equivalent amounts of **L1** and $Hg(ClO_4)_2$ compared to the calculated (Mercury 3.3) powder pattern for **4** (orange).

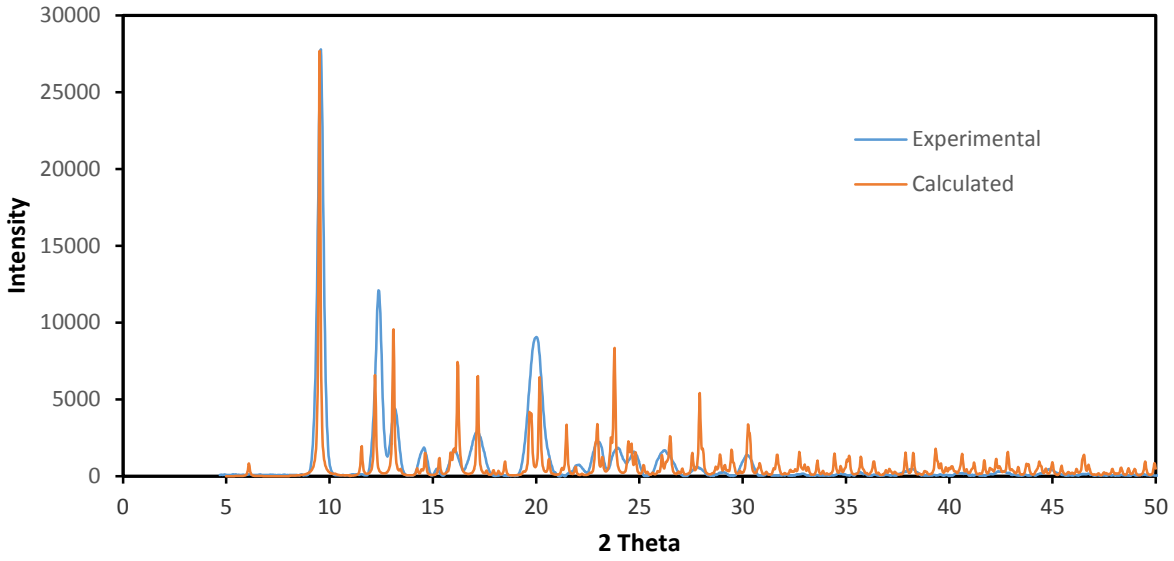

Figure S6. Powder diffraction analysis of precipitated [Cd(**L1**)(OH_2)($OClO_3$)](ClO_4) (**2**). Experimental data (blue) for the precipitate isolated following addition of m-xylene to a room temperature acetonitrile solution containing stiochiometrically equivalent amounts of **L1** and $Cd(ClO_4)_2$ compared to the calculated (Mercury 3.3) powder pattern for **2** (orange).

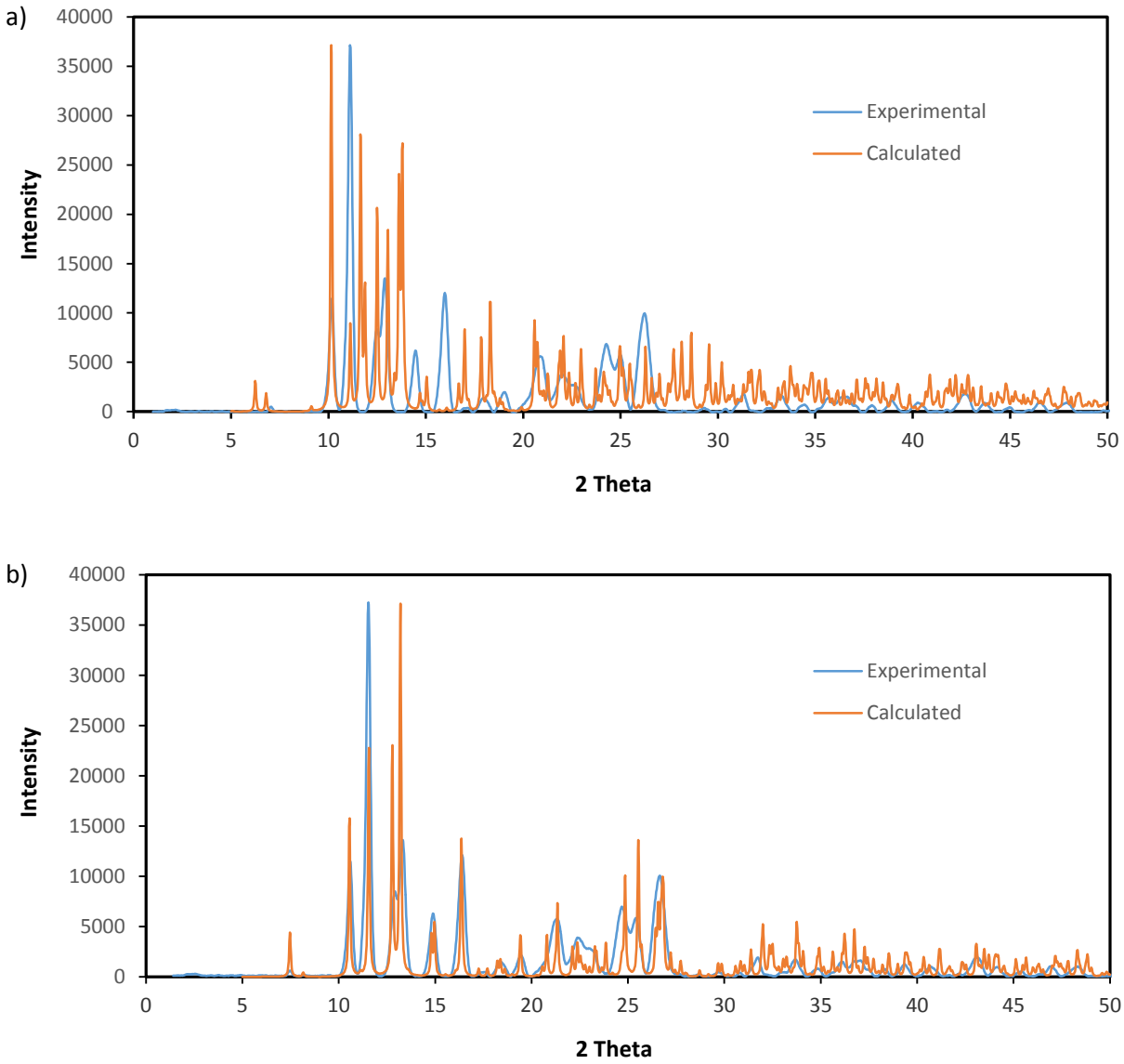

Figure S7. Powder diffraction analysis of precipitated [Hg(**L1**)$(ClO_4)_2$]. Experimental data (blue) for the precipitate isolated following addition of m-xylene to a room temperature acetonitrile solution containing stiochiometrically equivalent amounts of **L1** and $Hg(ClO_4)_2$ is compared to the calculated (orange, Mercury 3.3) powder pattern for a) **3** with calculated 2θ peaks at 11.66, 11.88, 13.64, and 13.78° poorly accounted for by experimental data and b) **4** with all calculated 2θ peaks reasonably well matched.

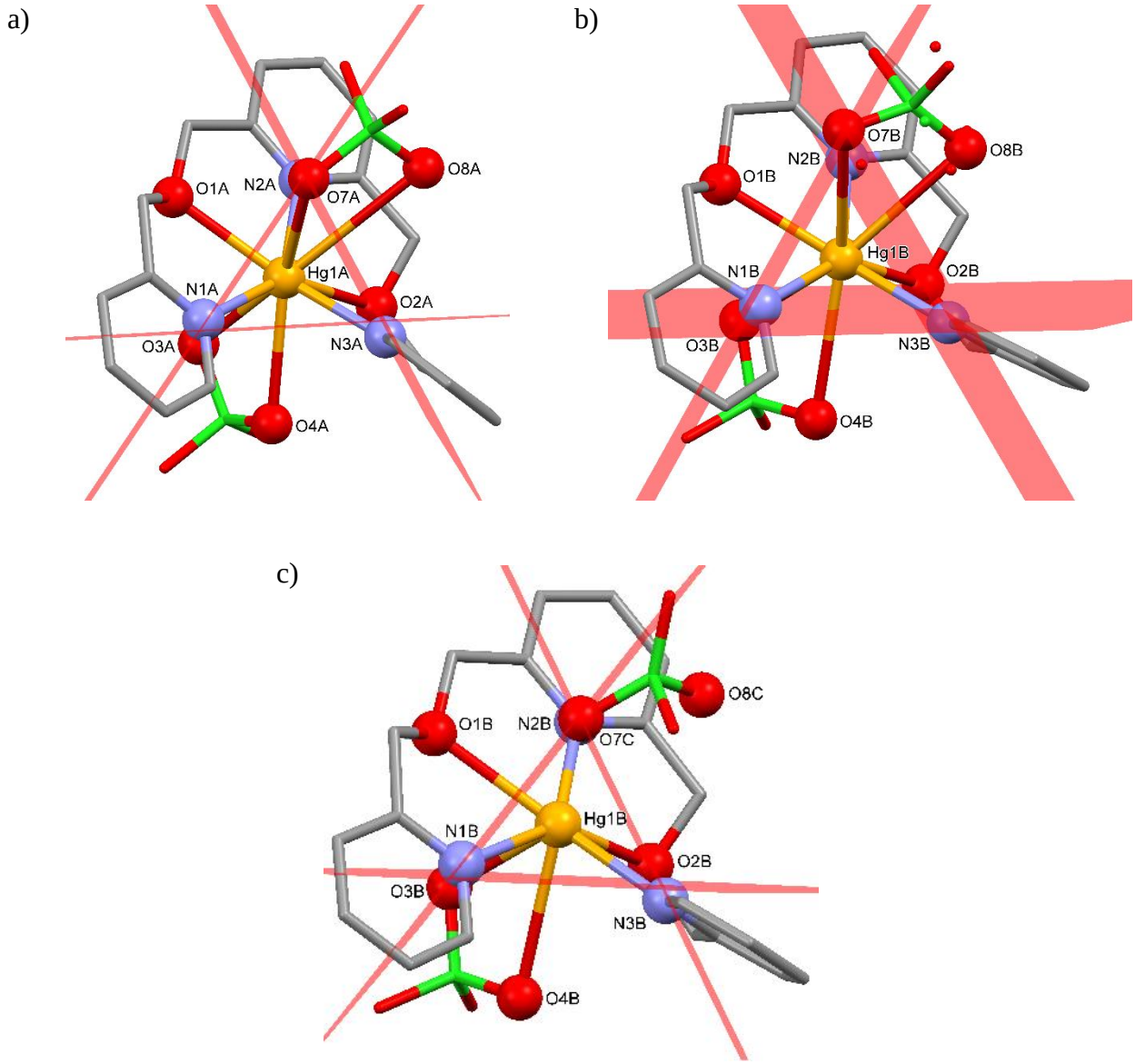

Figure S8. Overview of tricapped trigonal prismatic Hg(II) coordination geometry found in the independent molecules of **3** viewed down the pseudo three fold axis. a) Ordered Hg1A molecule. The angles between the square planes highlighted are 52.84°, 62.28° and 64.88°. The angle between the triangular planes is 11.37°. b) Hg1B with the Cl2B perchlorate position. The angles between the rectangular planes are 58.35°, 60.00° and 62.17°. The angle between the triangular planes is 11.37°. c) Square planes associated with the square antiprism coordination geometry of Hg1B with the Cl2C perchlorate position (Hg1B-O7C and Hg1B-O8c bonds not shown). The angles between the square planes highlighted are 53.83°, 61.75° and 64.46°. The angle between the triangular planes is 10.88°.

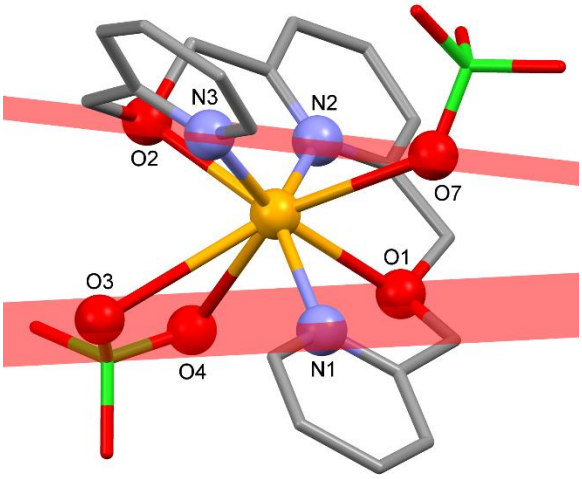

Figure S9. Overview of the square planes associated with the distorted square antiprism coordination geometry of **4**. The angle between the N2-N3-O2-O7 (rmsd 0.024) and N1-O1-O3-O4 (rmsd 0.17) planes is 10.07(13)°. Tethering constraints of the pentadentate ligand can account for both displacement of O1 from the N1-O1-O3-O4 ligand plane and tilting of this plane towards the other. The closely related dodecahedral coordination geometry would be expected to have these two square faces undergo orthogonal puckering towards two triangles.

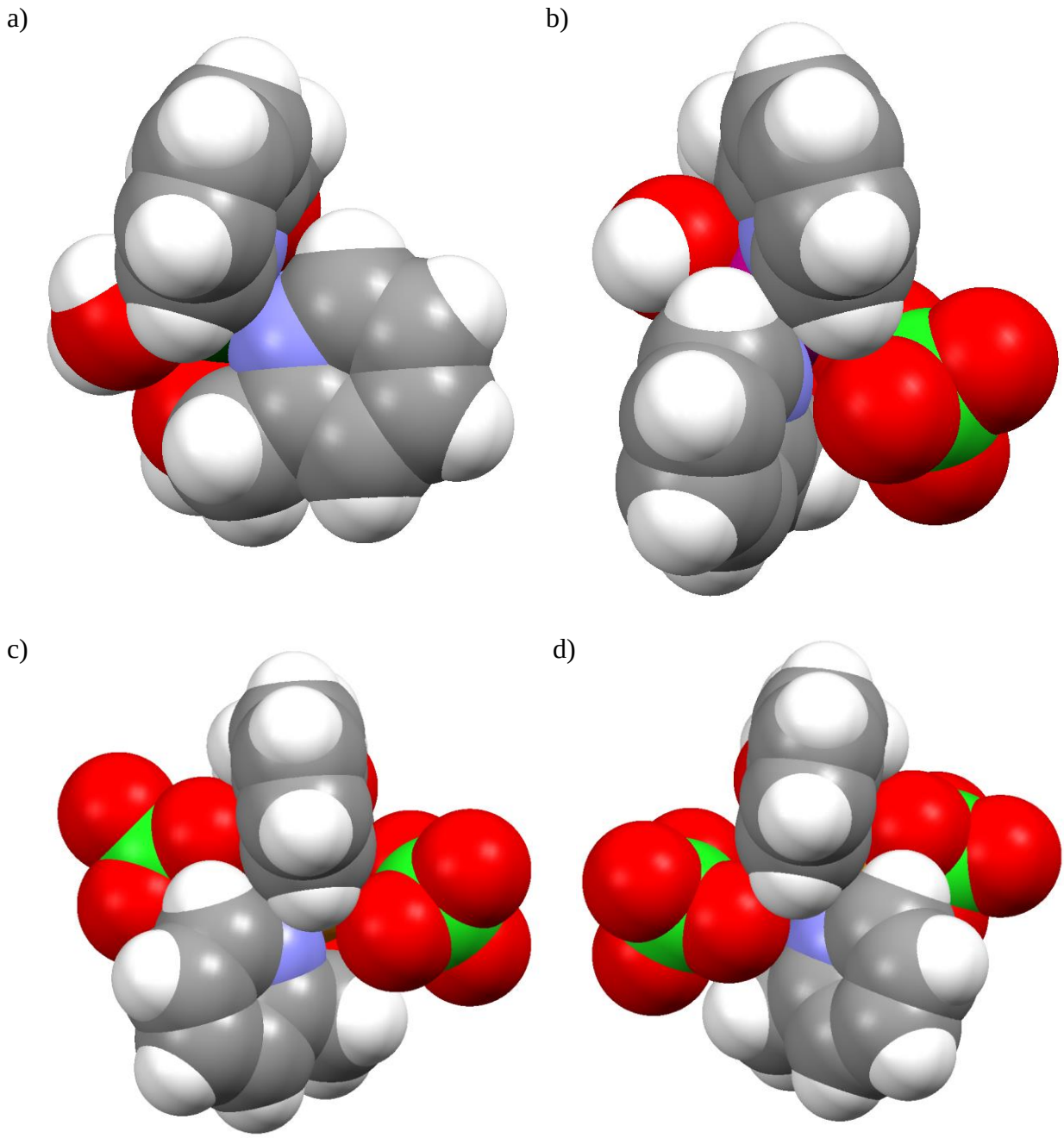

Figure S10. Spacefill views of $[Zn(\mathbf{L1})(OH_2)]^{2+}$ (cation of **1**), $[Cd(\mathbf{L1})(OH_2)(OClO_3)]^{+}$ (cation of **2**), **3** (one independent molecule) and **4** with the N2 pyridyl ring oriented approximately perpendicular to the page to highlight the conformational exposure of H_a to the shielding ring current of one of the other pyridyl rings.

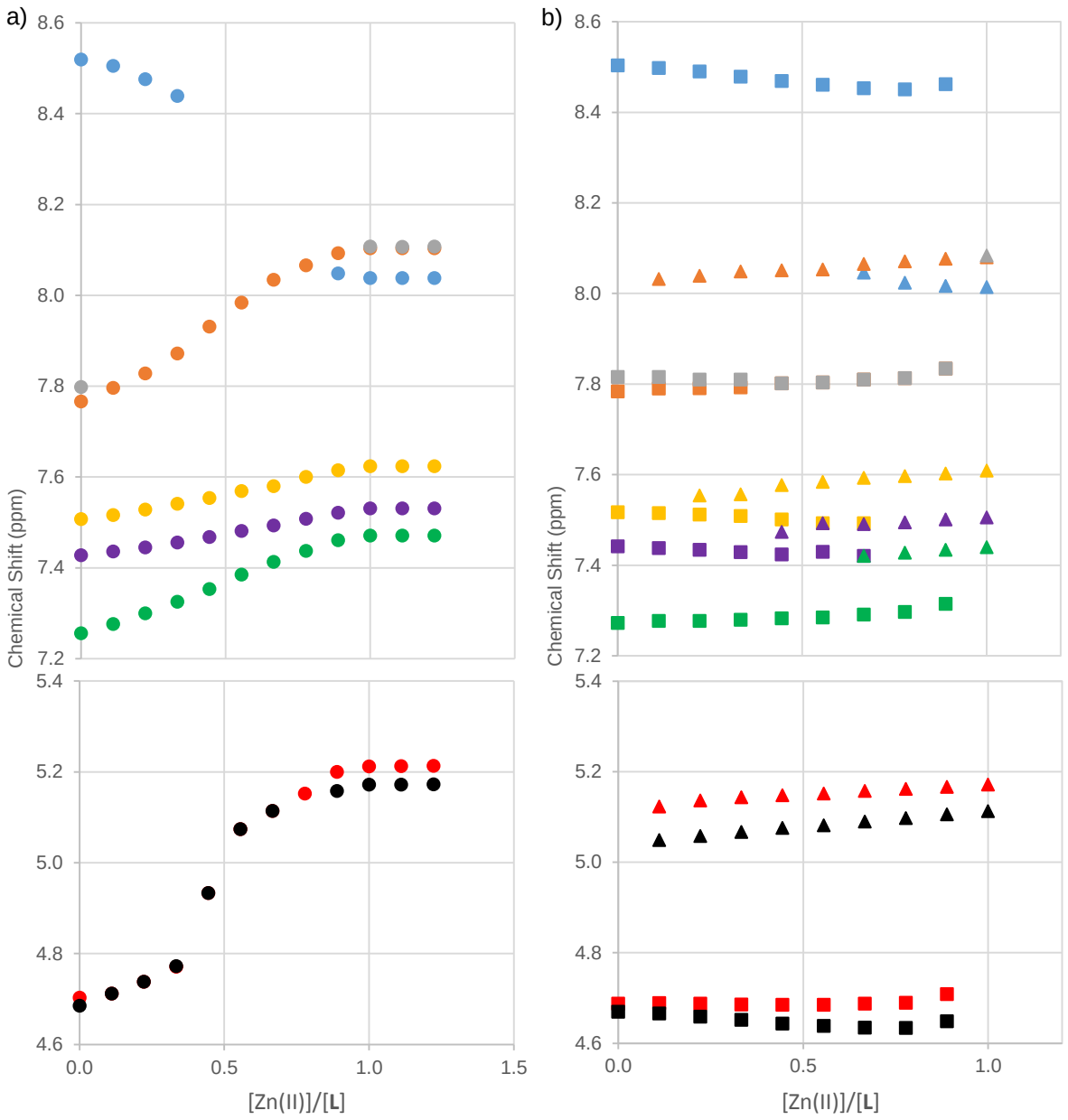

Figure S11. Plots of δ_H as a function of nominal $[Zn(ClO_4)_2{\cdot}6H_2O]/[\mathbf{L1}]$ with color coded proton assignments H_a, H_b, H_c, H_d, H_e, H_f, H_g and H_h at a) 20 °C and b) -40 °C. Squares are for exchange averaged δ_H closely associated with free **L1**. Triangles are for exchange averaged δ_H closely associated with $[M(\mathbf{L1})]^{2+}$. In some spectra, H_c and H_h were indistinguishable.

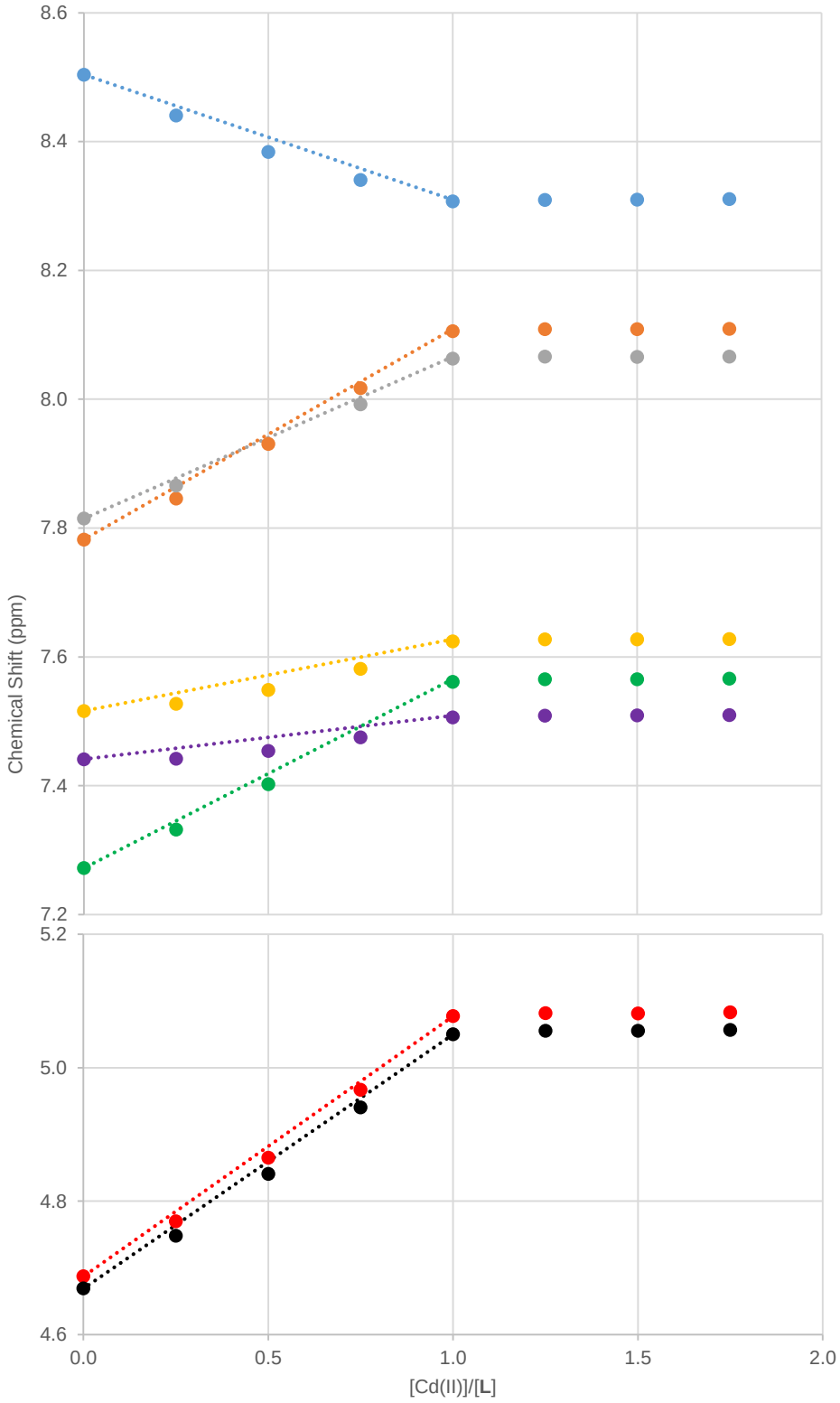

Figure S12. Plots of δ_H as a function of nominal $[Cd(ClO_4)_2 \cdot 6H_2O]$/[**L1**] at -40 °C in CD_3CN. Color code for proton assignments: H_a, H_b, H_c, H_d, H_e, H_f, H_g and H_h.